# Introduction of a $C_6D_6$ detector system on the Back-n of CSNS

*Jie* Ren[1,*], *Xichao* Ruan[1], *Jie* Bao[1], *Guangyuan* Luan[1], *Hanxiong* Huang[1], *Yangbo* Nie[1]

[1]Key Laboratory of Nuclear Data, China Institute of Atomic Energy, Beijing 102413, China

**Abstract:** Radiative neutron capture cross sections are very important in the field of basic physics research and nuclear device R&D. The Back-n white neutron beam line of China Spallation Neutron Source (CSNS) is the first spallation neutron beam line in China. On the purpose for radiative neutron capture cross section measurement, a $C_6D_6$ detector system was built in the Back-n experimental station. The pulse height weighting technique (PHWT) was used to make the system's detective efficiency independent of the cascade path and the energy of cascade gamma rays. The neutron energy spectrum was measured for the energy between 1eV and 80keV with a $^6$Li loaded ZnS scintillation detector. Besides, a testing experiment with $^{197}$Au and $^{169}$Tm samples was carried out to examine this system. According to the preliminary results, this $C_6D_6$ detector system can be used to perform neutron capture cross section measurement.

**Keywords:** $C_6D_6$ detector; PHWT; neutron capture cross section; white neutron source;

## 1. Introduction

Radiative neutron capture cross-section ($\sigma_{n\gamma}$) is one of the very important nuclear data in the field of the R&D of Accelerator Driven Systems (ADS), the transmutation of nuclear waste [1] and Nuclear Astrophysics. In the recent years, a lot of accurate $\sigma_{n\gamma}$ of important nuclides were measured based on the white neutron source facilities, such as the CERN n-TOF, GELINA, LANSCE and so on [2-4]. The Back-n of China Spallation Neutron Source (CSNS) is the first white neutron source in China that can provide neutron beam in the energy region between thermal neutron and hundreds MeV [5]. Many kinds of nuclear data measurements can be done with the Back-n, including the $\sigma_{n\gamma}$ measurement.

The $C_6D_6$ liquid scintillation detectors [6] are widely used for $\sigma_{n\gamma}$ measurements on time-of-flight facilities, because of its low neutron sensitivity and good time response. Besides, the pulse height weighting technique (PHWT) can be involved to make the efficiency independent of the cascade paths and the energy distribution of the cascade gamma rays [7]. A $C_6D_6$ detector system with four detectors has been installed at Back-n. The main purpose of this system is to perform $\sigma_{n\gamma}$ measurement, especially in the resonance energy region.

## 2 The Back-n of CSNS

The China Spallation Neutron Source (CSNS) is the first spallation neutron facility in China [8]. As shown in Fig.1, the incident proton beam of CSNS was deflected 15 degrees by a bending magnet at 24 m away from the spallation target [5]. Therefore, a neutron beam line, Back-n as known, can be built in the 180 degree direction by sharing a common vacuum tube with the proton beam line. The Back-n can provide pulsed white neutron beam with energy from thermal to 400 MeV, and the neutron flux can reach to $10^7$ $cm^{-2}s^{-1}$ at the experimental stations [9]. The accelerator can be operated in double-bunch mode or in single-bunch mode. With the single-bunch mode, the neutron time resolution is about 0.8% in the energy region between 1 eV and 1 MeV at 80 m from the spallation target [10]. The Back-n beam line has two experimental stations: ES#1 located at 56 m from the spallation target and ES#2 at 76 m.

* Corresponding author: renjie@ciae.ac.cn

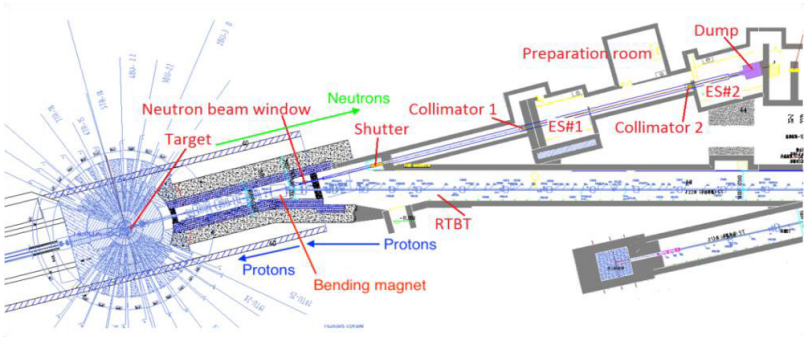


**Fig.1** Layout of Back-n beam line at CSNS

Neutron spectrum at the experimental stations was measured with a multi-layer fission chamber (MFC) [11, 12]. The MFC was developed by China Institute of Atomic Energy and the neutron converters were $^{235}$U and $^{238}$U. However, the neutron spectrum measured by MFC is not sufficiently accurate for this energy region between 1 eV and 20 keV. $^{235}$U used as neutron converter in the MFC has lots of resonances in this region, and the fission cross section of $^{235}$U in the resonance region is not a standard cross section. Therefore, another neutron spectrum measurement was carried out with $^{6}$Li-loaded ZnS scintillation detector.

The $^{6}$Li-loaded ZnS scintillator used in the neutron spectrum measurement was EJ-420, produced by ELJEN Technology Corporation, with 50 mm in diameter and 6 mm thick. It was set in the EH#2 of the Back-n, 76.9 m away from the spallation target. The anode signal of the photomultiplier tube (PMT) was delivered to DT5730B, a digitizer made by CAEN with 500 MS/s sample rate and 14 bit resolution. The digitized waveforms were stored and the data reduction was performed off-line.

As most of the scintillators are sensitive to both of the neutron and gamma rays, the pulse shape discrimination (PSD) is very important in the data reduction. Fig.2 shows a neutron waveform (red triangle) and a gamma waveform (black square). The decay time of the neutron waveforms are much longer than those of the gamma rays. So the neutron waveforms can be separated with the gamma rays' by comparing their tails in the PSD routine.

The incident neutron energy was determined via time of flight (TOF) method. In this work , the time of the waveforms were measured by a internal clock of the DT5730B. The gamma-flash which was from the impact of the proton pulse on the spallation target was used as the time reference. With about $10^6$ gamma rays arriving at almost the same time, the signal of the gamma-flash is much larger than the single particle's signal, thus it can be easily distinguished and used as the start time ($tof_\gamma$) of each proton beam pulse. The neutron arrive time ($tof_n$) can be get from its waveform. Then the real flight time of neutron ($tof_n'$) can be determined with

$$tof_n' = (tof_n - tof_\gamma) + L/c \quad , \qquad (1)$$

where L is the length of the flight path and c is the speed of light. The neutron energy spectrum of EJ-420 and that of the MFC are shown in Fig.3, with 40 bins per decade (bpd) with energy logarithmic scale. Obviously, the spectrum is not smooth in the region between 1 eV and 80keV. The resonance energies of the spallation target materials can be recognized in the neutron spectrum, such as 4.28 eV of $^{181}$Ta, 10.19eV of $^{184}$W, 21.07eV of $^{182}$W, 132.0eV of $^{59}$Co and so on. This may be a drawback of the Back-n for resonance parameters analysis. However, this neutron energy spectrum is still not sufficient enough because the absolute neutron detective efficiency of EJ-420 is not well known. Another measurement will be performed with an accurate quantitative $^{6}$Li or $^{10}$B ionization chamber in the next step.

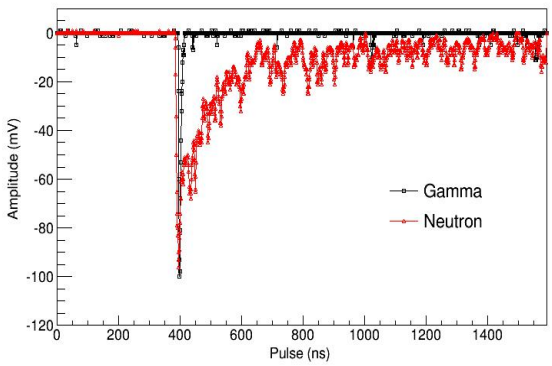


**Fig.2** Waveforms of the EJ-420 detector: neutron waveform (red triangle) and gamma waveform (black square)

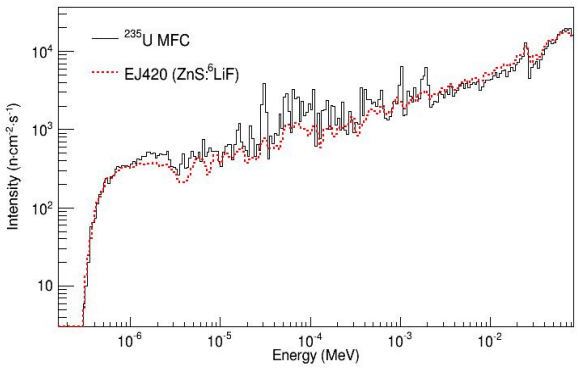


**Fig.3** Neutron energy spectrum between 1.0 eV and 80.0 keV: energy spectrum of MFC (black solid line), energy spectrum of EJ-420 ( red dotted line).

## 3 The $C_6D_6$ detector system of Back-n

### 3.1 System configuration

The Back-n $C_6D_6$ detector system consists of four $C_6D_6$ detectors and aluminium detector and sample holders [13], as shown in Fig.4. The $C_6D_6$ detectors are placed upstream of the sample relative to the neutron beam, and the detector axis is at an angle of 110 degrees with respect to the neutron beam direction. The distance from the centre of the front face of the detector to the neutron beam centre is about 80 mm, and the distance between the detector centre and the sample centre is about 150 mm. The $C_6D_6$ liquid scintillator is EJ-315, which is also produced by ELJEN Technology Corporation. The 130 mm in diameter and 76.2 mm long shell of the scintillator is made of aluminium. The PMT coupled to the scintillator is ETEL 9390KEB, with borosilicate window and covered by mu metal and an aluminium shell.

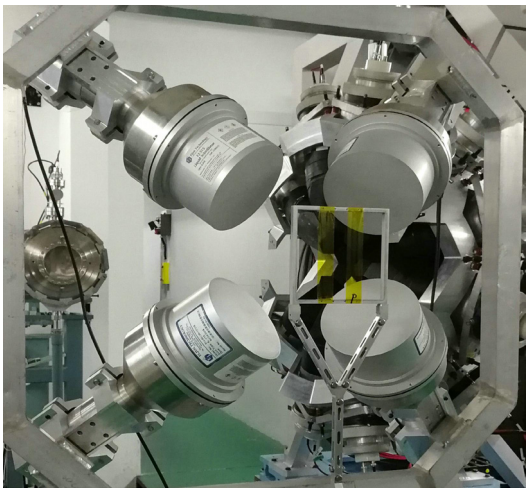

**Fig.4** Photo of the $C_6D_6$ detector system

The response of the $C_6D_6$ detector to gamma rays is very important for the $\sigma_{n\gamma}$ measurement. Three different radioactive sources, $^{137}Cs$, $^{22}Na$ and $^{238}Pu/^{13}C$ sources with gamma ray energies of 662 keV, 511 keV &1.27 MeV, and 6.13 MeV respectively, were used to calibrate the energy deposition of the $C_6D_6$ detectors [13]. Geant4 code [14] was used to simulate the response of the $C_6D_6$ detector to the mono-energetic gamma rays above. The instrumental resolution at a certain energy, which is assumed to be a Gaussian, can be determined by convoluting the simulation spectrum to fit the experimental spectrum, as described in the section 4.4 of reference [15]. Fig.5 shows a good linear relationship between the maximum energy of Compton electron and the pulse height value (PH) of the deposition energy. Fig.6 shows the energy resolution of one $C_6D_6$ detector.

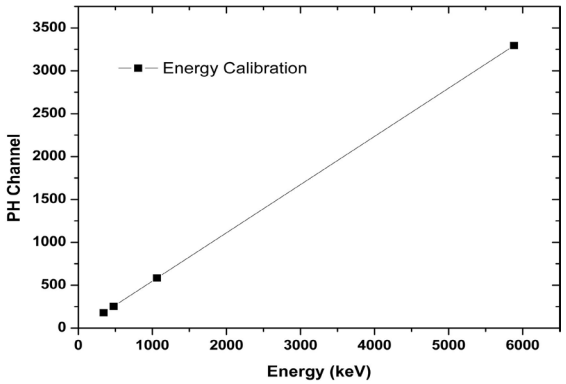


**Fig.5** The fitting result of the deposited energy calibration

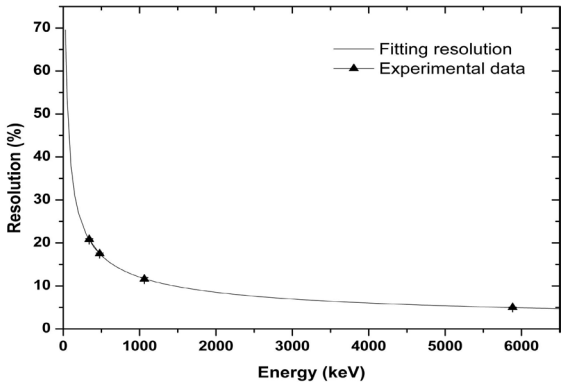


**Fig.6** Energy resolution of one $C_6D_6$ detector

The weighting function $W(E_{dep})$ of the PHWT is defined such that it follows the relationship [16]:

$$\int_{E_L}^{\infty} R_{dep}(E_{dep}, E_\gamma) W(E_{dep}) dE_{dep} = \eta E_\gamma \quad . \tag{2}$$

The $R_{dep}$ is the detector's response to a gamma ray with energy $E_\gamma$. The $E_L$ is the energy threshold of the $E_{dep}$, and the proportionality factor $\eta$ is usually taken equal to 1 $MeV^{-1}$ when deriving $W(E_d)$. According to reference [16], the weighting function can be approximated by a polynomial function

$$WF_i = \sum_{k=0}^{4} a_k E_i^k \quad , \tag{3}$$

where $E_i$ designates the energy of bin i in the response function and $a_k$ is a coefficient which has energy inverse units to the power of k. The weight function can be determined by the least squares minimization

$$\chi^2 = \sum_{j=1}^{26} \left( \sum_{i=1}^{1200} \sum_{k=0}^{4} a_k ((i-0.5)\Delta E)^k R_i^j - \eta E_{\gamma j} \right)^2 \quad . \tag{4}$$

The i is the bin of the deposited energy histogram, the j denotes how many groups of mono-energetic gamma rays were used in the simulation and the $\eta$ is usually equal to 1 $MeV^{-1}$. Geant4 code was used to calculate the response distributions of the $C_6D_6$ detector to mono-energetic gamma ray ejected isotropically from a 0.2 mm $^{197}Au$ disc. Fig.7 shows the weighting function. The weighted detective efficiency should be equal to $E_\gamma$, as shown in Fig.8.

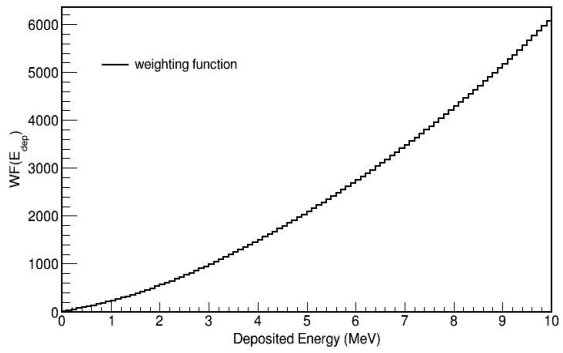


**Fig.7** The weighting function of the $C_6D_6$ detector for 0.2 mm thick $^{197}$Au disc.

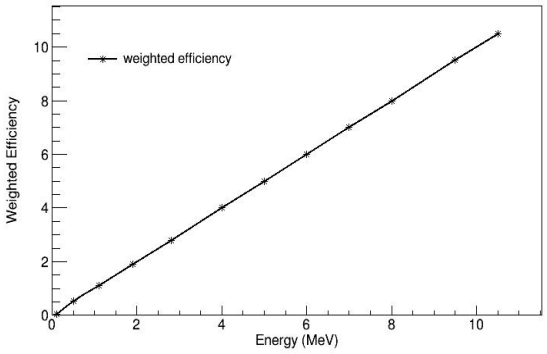


**Fig.8** The weighted detective efficiency of the $C_6D_6$ detector.

### 3.2 Experimental testing of the $C_6D_6$ detector system

An experiment to test the $C_6D_6$ detector system was carried out at the ES#2 of Back-n. Four $C_6D_6$ detectors were placed at about 76.6 m away from the centre of the spallation target. Anode signals delivered by the PMTs were registered by the readout electronics [17], which can digitize the analog signals into full waveform data with 1 GS/s sampling rate and 12 bit resolution. The $^{197}$Au, $^{169}$Tm samples were used in this experiment. Table.1 gives the characteristics of these samples.

**Table 1** Samples used in this experiment

| Sample | Diameter (mm) | Thickness (mm) | Purity (%) |
|---|---|---|---|
| $^{197}$Au | 40.0 | 0.2 | 99.99 |
| $^{169}$Tm | 40.0 | 0.2 | 99.99 |

The neutron intensity was monitored by a $^{6}$Li-Si detector [12] and by the proton beam intensity. The counting rates of the two monitoring systems were compared to minimise the systematic uncertainty of the neutron intensity.

Incident neutron energy is related with flight time and flight path by means of the relationship

$$E_n = \left(\frac{72.2977(L_0 + \Delta L)}{t}\right)^2 , \quad (5)$$

where $E_n$ is the neutron energy (MeV), $L_0$ is the geometrical distance between the centre of the CSNS target and the sample, 76.61 ± 0.01 m according to the GPS measurement , ΔL is the moderation path (m) [18], and t is the time of flight (ns).

There were three kinds of signals recorded by the readout electronics. The first one is the signal of the proton beam bunch, which is delivered by a Faraday tube on the proton beam line and used as the trigger of the digitizer. The second one is the signal of the gamma-flash, which was used as the time reference as mentioned in section 2. The third are the single particle signals induced by cascade gamma rays, scattering gamma rays, scattering neutron and so on. In one proton pulse cycle, there was one gamma flash signal followed by dozens of single particle signals. All the signals were timed by the main clock of the readout electronics. The flight time t was also determined with Eq.1, where $tof_n$ was the time of the single particle signal, and the $tof_\gamma$ was the time of the gamma-flash. Fig.9 shows the TOF spectrum of $^{197}$Au.

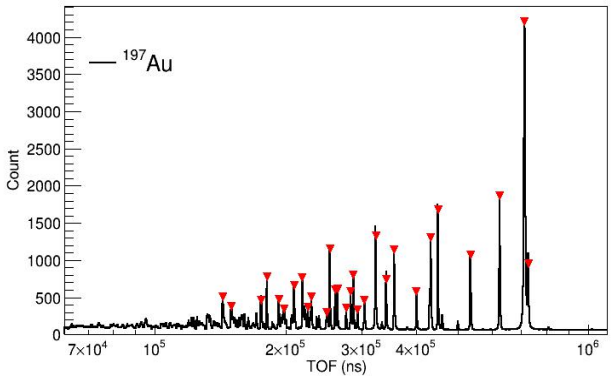


**Fig.9** The TOF spectrum of the $^{197}$Au sample.

The neutron capture resonance energies known with high precision can be used to determine the moderation path length ΔL. In this work, the resonance energies of $^{197}$Au in BVIII.0 [19] were used to get ΔL. In Fig.9 the resonance peaks were picked up and then the effective flight length L can be determined with

$$L = t \cdot \sqrt{E_n} / 72.2997 , \quad (6)$$

where $E_n$ was the resonance energies. Then the ΔL at the resonance energy can be obtained with

$$\Delta L = L - L_0 . \quad (7)$$

A polynomial function (Eq.8) was be used to fit the ΔL, as shown in Fig.10.

$$\Delta L = \sum_{k=-1}^{2} a_k E_n^k . \quad (8)$$

The $L_0$ is defined as the distance between the centre of the spallation target and the centre of the sample, so the minus ΔL means that the neutron was produced in the first half of the target.

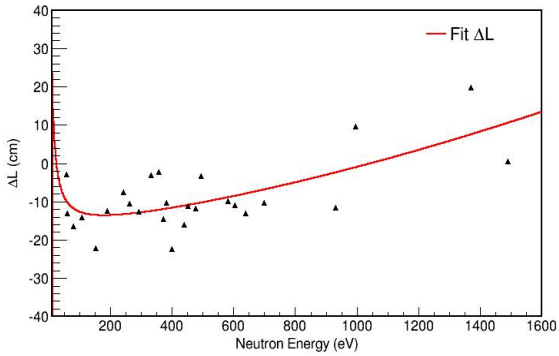


**Fig.10** The ΔL at the resonance energies of the $^{197}$Au sample. The red solid line is the fitting results with Eq.8.

The main sources of the ΔL uncertainty are from the uncertainties of the flight time and the geometrical flight path length $L_0$. The accelerator was operated in double bunches mode during this experiment. The time interval of the two beam bunch (410 ns) was the main source of the flight time deviation. The deviation of the $L_0$ is 1.0 cm according to the GPS measurement.

With the ΔL and TOF spectrum of $^{169}$Tm (shown as Fig.11), the resonance energies of $^{169}$Tm can be determined with Eq.5. The resonance energies of this work and that of BVIII.0 [19] are given in Table.2. The fist resonance energy of $^{169}$Tm is 3.906 eV, which corresponds to the peak around $3.0\times10^6$ ns in the TOF spectrum. However, this resonance is so large that the neutron capture yield is saturated at this energy for the 0.2 mm thick $^{169}$Tm. Therefore, the first resonance energy can't be obtained in this work.

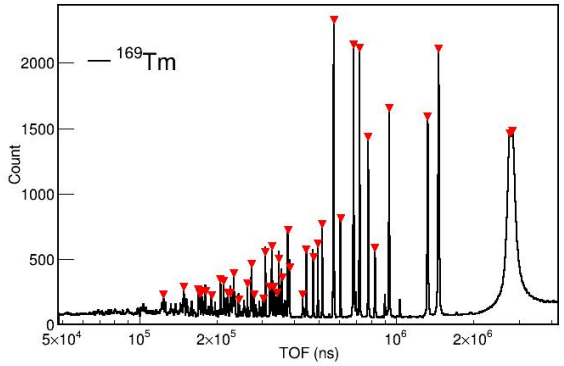


**Fig.11** The TOF spectrum of $^{169}$Tm

**Table.2** The experimental results and evaluated data of the $^{169}$Tm resonance energies

| **ENDF BVIII.0 (eV)** | **This work (eV)** | **$\Delta_\pm$ (%)** | **ENDF BVIII.0 (eV)** | **This work (eV)** | **$\Delta_\pm$ (%)** |
|---|---|---|---|---|---|
| 14.32 | 14.39 | 0.84 | 282.70 | 282.73 | 1.02 |
| 17.42 | 17.50 | 0.85 | 296.40 | 296.29 | 1.03 |
| 34.79 | 34.85 | 0.87 | 318.50 | 318.61 | 1.03 |
| 44.79 | 44.85 | 0.88 | 332.30 | 332.33 | 1.04 |
| 50.58 | 50.64 | 0.89 | 389.70 | 389.73 | 1.05 |
| 59.07 | 59.23 | 0.90 | 407.50 | 408.43 | 1.05 |
| 65.75 | 65.95 | 0.90 | 439.80 | 440.24 | 1.08 |
| 83.18 | 83.33 | 0.92 | 511.20 | 513.89 | 1.08 |
| 94.10 | 93.88 | 0.93 | 564.10 | 564.42 | 1.09 |
| 124.80 | 124.90 | 0.95 | 597.90 | 597.10 | 1.12 |
| 135.60 | 135.56 | 0.96 | 623.70 | 625.77 | 1.14 |
| 153.00 | 153.10 | 0.97 | 676.20 | 674.55 | 1.15 |
| 163.80 | 163.85 | 0.97 | 714.30 | 713.62 | 1.15 |
| 207.00 | 207.07 | 1.00 | 840.00 | 839.06 | 1.17 |
| 213.30 | 213.47 | 1.00 | 937.30 | 934.76 | 1.18 |
| 250.80 | 250.31 | 1.02 | 1034.00 | 1038.98 | 1.21 |
| 259.50 | 259.87 | 0.84 | 1065.00 | 1063.69 | 1.24 |
| 273.00 | 272.97 | 0.85 | 1381.00 | 1384.21 | 1.26 |

The sources of the energy uncertainty are mainly from the uncertainties of the flight time and flight path length. The uncertainty of the flight time is also from the time interval of the two proton bunches. The uncertainty of the flight path is less than 0.3% according to the uncertainty of the $L_0$ an ΔL.

Since the neutron flux in resonance energy region is not known accurately enough at the moment, the resonance parameters analysis as well as calculating the $\sigma_{n\gamma}$ are difficult and therefore still in progress. Nevertheless, according to the preliminary experimental results, the neutron energy resolution of the measurements with this C6D6 detector system is sufficient for $\sigma_{n\gamma}$ measurements in the resonance energy region.

## 4 Conclusions

A $C_6D_6$ detector system has been built at the ES#2 of Back-n at CSNS. According to the first experimental results with $^{197}$Au and $^{169}$Tm sample, neutron resonance energies can be accurately determined. However, the neutron flux in the resonance energy region is still need to be measured more accurately. Then the resonance parameters analysis will be performed after that.

This work was supported by the National Natural Science Foundation of China (Grant Nos. 11790321 and Nos. 11805282) , National Key R&D Program of China (Grant Nos. 2016YFA0401601) and Continuous Basic Scientific Research Project (No. WDJC-2019-09).

## References

1. W.Maschek, X.Chen, F.Delage et al., Progress in Nuclear Energy 50(2), 333 (2008).

2. The n TOF Collaboration, The European Physical Journal Plus, 131(10):371 (2016).
3. D.Ene, C.Borcea, S.Kopecky, et al., Nuclear Instruments and Methods in Physics Research A, 618, 54 – 68 (2010).
4. Paul W.Lisowski, Kurt F.Schoenberg. Nuclear Instruments and Methods in Physics Research A, 562,910-914 (2006).
5. H.T.Jing, J.Y.Tang, H.Q.Tang, et al., Nuclear Instruments and Methods in Physics Research A, 621, 91-96 (2010).
6. F.Corvi, C.Bastian, K.Wisshak. Nucl. Sci. Eng., 93(4), 348 –358(1986).
7. J.N.Wilson, B.Haas, S.Boyer et al., Nuclear Instruments and Methods in Physics Research A, 511,388-399 (2003).
8. H. Chen , X.L.Wang, Nature Materials, 15(7), 689-691 (2016).
9. J.Y.Tang, S.N.Fu, H.T.Jing, et al., Chinese Physics C, 34,121-125(2010).
10. Q.An, H.Y.Bai, J.Bao, et al., Journal of Instrumentation, 12, 7-22(2017).
11. Y.H.Chen, G.Y.Luan, J.Bao, et al., Eur.Phys.J.A, 55(7):115 (2019).
12. J.Bao, Y.H.Chen, X.P.Zhang, et al. Acta Physica Sinica, 68(8) (2019) (in Chinese).
13. J.Ren, X.C.Ruan, J.Bao, et al, Radiation Detection Technology and Methods, 3:52 (2019).
14. Geant4 Collaboration, GEANT4 User's Guide for Application Developers (version: 10.2), http://geant4.cern.ch.
15. C.Domingo-Pardo, PhD.thesis, CSIC-University of Valencia, 2005.
16. J.L. Tain, F.Gunsing, D.Cano, et al., Jour. of Nucl. Sci. and Tech., 39,689-692 (2002).
17. Q. Wang, P.Cao, X.Qi et al., Review of Scientific Instruments, 89,013511 (2018).
18. C. Guerrero, et al., Eur. Phys. J. A, 49: 27, (2013).
19. D.A. Brown *et al.*, Nucl. Data Sheets **148**, 1 (2018).